The Astrophysical Journal Letters, 945:L23 (8pp), 2023 March 10 https://doi.org/10.3847/2041-8213/acbf45

Simultaneous Millimeter-wave, Gamma-Ray, and Optical Monitoring of the Blazar PKS 2326-502 during a Flaring State

J. C. Hood II[1,2,3], A. Simpson[4], A. McDaniel[5], A. Foster[6], P. A. R. Ade[7], M. Ajello[5], A. J. Anderson[8], J. E. Austermann[9,10], J. A. Beall[9], A. N. Bender[1,11], B. A. Benson[1,2,8], F. Bianchini[12], L. E. Bleem[1,11], J. E. Carlstrom[1,2,11,13,14], C. L. Chang[1,2,11], P. Chaubal[12], H. C. Chiang[15,16], T-L. Chou[1,13], R. Citron[17], C. Corbett Moran[18], T. M. Crawford[1,2], A. T. Crites[1,2,19,20], T. de Haan[21,22], M. A. Dobbs[15,23], W. Everett[24], J. Gallicchio[1,25], E. M. George[26,27], N. Gupta[28], N. W. Halverson[10,24], G. C. Hilton[9], G. P. Holder[23,29,30], W. L. Holzapfel[27], J. D. Hrubes[17], N. Huang[27], J. Hubmayr[9], K. D. Irwin[31,32], L. Knox[33], A. T. Lee[27,34], D. Li[9,31], A. Lowitz[2], G. Madejski[35], M. Malkan[36], J. J. McMahon[1,2,13], S. S. Meyer[1,2,13,14], J. Montgomery[15], T. Natoli[1,2], J. P. Nibarger[9], G. Noble[15], V. Novosad[37], Y. Omori[32], S. Padin[1,2,38], S. Patil[12], C. Pryke[39], C. L. Reichardt[12], J. E. Ruhl[6,40], B. R. Saliwanchik[41,42], K. K. Schaffer[1,14,43], C. Sievers[17], G. Smecher[15,44], A. A. Stark[45], C. Tucker[7], T. Veach[46], J. D. Vieira[29,30,47], G. Wang[11], N. Whitehorn[48], W. L. K. Wu[1,31], V. Yefremenko[11], J. A. Zebrowski[27], and L. Zhang[49,50,51]

[1] Kavli Institute for Cosmological Physics, University of Chicago, 5640 South Ellis Avenue, Chicago, IL 60637, USA; hood.astro@gmail.com
[2] Department of Astronomy and Astrophysics, University of Chicago, 5640 South Ellis Avenue, Chicago, IL 60637, USA
[3] Department of Physics and Astronomy, Vanderbilt University, Nashville, TN 37235, USA
[4] Department of Physics, Rensselaer Polytechnic Institute, Troy, NY 12180, USA
[5] Department of Physics and Astronomy, Clemson University, Clemson, SC 29631, USA
[6] Department of Physics, Case Western Reserve University, Cleveland, OH 44106, USA
[7] Cardiff University, Cardiff CF10 3XQ, UK
[8] Fermi National Accelerator Laboratory, MS209, P.O. Box 500, Batavia, IL 60510, USA
[9] NIST Quantum Devices Group, 325 Broadway Mailcode 817.03, Boulder, CO 80305, USA
[10] Department of Physics, University of Colorado, Boulder, CO 80309, USA
[11] High Energy Physics Division, Argonne National Laboratory, 9700 S. Cass Avenue, Argonne, IL 60439, USA
[12] School of Physics, University of Melbourne, Parkville, VIC 3010, Australia
[13] Department of Physics, University of Chicago, 5640 South Ellis Avenue, Chicago, IL 60637, USA
[14] Enrico Fermi Institute, University of Chicago, 5640 South Ellis Avenue, Chicago, IL 60637, USA
[15] Department of Physics, McGill University, 3600 Rue University, Montreal, Quebec H3A 2T8, Canada
[16] School of Mathematics, Statistics & Computer Science, University of KwaZulu-Natal, Durban, South Africa
[17] University of Chicago, 5640 South Ellis Avenue, Chicago, IL 60637, USA
[18] TAPIR, Walter Burke Institute for Theoretical Physics, California Institute of Technology, 1200 E California Blvd., Pasadena, CA, 91125, USA
[19] Dunlap Institute for Astronomy & Astrophysics, University of Toronto, 50 St George Street, Toronto, ON, M5S 3H4, Canada
[20] Department of Astronomy & Astrophysics, University of Toronto, 50 St George Street, Toronto, ON, M5S 3H4, Canada
[21] Institute of Particle and Nuclear Studies (IPNS), High Energy Accelerator Research Organization (KEK), Tsukuba, Ibaraki 305-0801, Japan
[22] International Center for Quantum-field Measurement Systems for Studies of the Universe and Particles (QUP), High Energy Accelerator Research Organization (KEK), Tsukuba, Ibaraki 305-0801, Japan
[23] Canadian Institute for Advanced Research, CIFAR Program in Gravity and the Extreme Universe, Toronto, ON, M5G 1Z8, Canada
[24] Department of Astrophysical and Planetary Sciences, University of Colorado, Boulder, CO 80309, USA
[25] Harvey Mudd College, 301 Platt Blvd., Claremont, CA 91711, USA
[26] European Southern Observatory, Karl-Schwarzschild-Str. 2, D-85748 Garching bei München, Germany
[27] Department of Physics, University of California, Berkeley, CA 94720, USA
[28] CSIRO Space & Astronomy, PO Box 1130, Bentley WA 6102, Australia
[29] Astronomy Department, University of Illinois at Urbana-Champaign, 1002 W. Green Street, Urbana, IL 61801, USA
[30] Department of Physics, University of Illinois Urbana-Champaign, 1110 W. Green Street, Urbana, IL 61801, USA
[31] SLAC National Accelerator Laboratory, 2575 Sand Hill Road, Menlo Park, CA 94025, USA
[32] Dept. of Physics, Stanford University, 382 Via Pueblo Mall, Stanford, CA 94305, USA
[33] Department of Physics, University of California, One Shields Avenue, Davis, CA, 95616, USA
[34] Physics Division, Lawrence Berkeley National Laboratory, Berkeley, CA 94720, USA
[35] Kavli Institute for Particle Astrophysics and Cosmology, SLAC National Accelerator Laboratory, Menlo Park, CA 94025, USA
[36] Department of Physics and Astronomy, University of California, Los Angeles, CA 90095-1547, USA
[37] Materials Sciences Division, Argonne National Laboratory, 9700 S. Cass Avenue, Argonne, IL 60439, USA
[38] California Institute of Technology, 1200 E. California Blvd., Pasadena CA 91125, USA
[39] School of Physics and Astronomy, University of Minnesota, 116 Church Street S.E. Minneapolis, MN 55455, USA
[40] Center for Education and Research in Cosmology and Astrophysics, Case Western Reserve University, Cleveland, OH 44106, USA
[41] Physics Department, Center for Education and Research in Cosmology and Astrophysics, Case Western Reserve University, Cleveland, OH 44106, USA
[42] Department of Physics, Yale University, P.O. Box 208120, New Haven, CT 06520-8120, USA
[43] Liberal Arts Department, School of the Art Institute of Chicago, 112 S Michigan Avenue, Chicago, IL 60603, USA
[44] Three-Speed Logic, Inc., Victoria, B.C., V8S 3Z5, Canada
[45] Harvard-Smithsonian Center for Astrophysics, 60 Garden Street, Cambridge, MA 02138, USA
[46] Space Science and Engineering Division, Southwest Research Institute, San Antonio, TX 78238, USA
[47] Center for AstroPhysical Surveys, National Center for Supercomputing Applications, Urbana, IL 61801, USA
[48] Department of Physics and Astronomy, Michigan State University, 567 Wilson Road, East Lansing, MI 48824, USA
[49] Department of Physics, University of California, Santa Barbara, CA 93106, USA
[50] Department of Physics, University of Illinois at Urbana-Champaign, 1110 West Green Street, Urbana, IL 61801, USA

[51] Department of Astronomy, University of Illinois at Urbana-Champaign, 1002 West Green Street, Urbana, IL 61801, USA
Received 2023 January 3; revised 2023 February 23; accepted 2023 February 26; published 2023 March 10

Abstract

Including millimeter-wave data in multiwavelength studies of the variability of active galactic nuclei (AGN) can provide insights into AGN physics that are not easily accessible at other wavelengths. We demonstrate in this work the potential of cosmic microwave background (CMB) telescopes to provide long-term, high-cadence millimeter-wave AGN monitoring over large fractions of sky. We report on a pilot study using data from the SPTpol instrument on the South Pole Telescope (SPT), which was designed to observe the CMB at arcminute and larger angular scales. Between 2013 and 2016, SPTpol was used primarily to observe a single 500 deg^2 field, covering the entire field several times per day with detectors sensitive to radiation in bands centered at 95 and 150 GHz. We use SPT 150 GHz observations to create AGN light curves, and we compare these millimeter-wave light curves to those at other wavelengths, in particular γ-ray and optical. In this Letter, we focus on a single source, PKS 2326-502, which has extensive, day-timescale monitoring data in gamma-ray, optical, and now millimeter-wave between 2013 and 2016. We find PKS 2326-502 to be in a flaring state in the first 2 yr of this monitoring, and we present a search for evidence of correlated variability between millimeter-wave, optical R-band, and γ-ray observations. This pilot study is paving the way for AGN monitoring with current and upcoming CMB experiments such as SPT-3G, Simons Observatory, and CMB-S4, including multiwavelength studies with facilities such as Vera C. Rubin Observatories Large Synoptic Survey Telescope.

Unified Astronomy Thesaurus concepts: Active galactic nuclei (16); Blazars (164); Millimeter astronomy (1061); Gamma-ray astronomy (628)

1. Introduction

Active galactic nuclei (AGN) are accreting supermassive ($M \gtrsim 10^5\ M_\odot$) black holes commonly found at the centers of massive galaxies (e.g., Kormendy & Richstone 1995; Gebhardt et al. 2000). The Unified Model of AGN proposes to explain observed categories of AGN via a scenario in which the appearance of a source depends on the angle between the axis of symmetry of the source and the line of sight of the observer (e.g., Antonucci 1993; Urry & Padovani 1995). For example, in this scenario, blazars—radio-loud AGN[52]—that also emit strongly in the γ-ray band are understood to have a relativistic jet pointed at relatively small angles (<5°) to the observer. The spectral energy distribution (SED) of blazars has a characteristic double-humped structure, with one peak located anywhere from the high-frequency radio to the soft X-ray band, caused by synchrotron emission from energetic electrons in the blazar jet, and a high-energy peak in the MeV–TeV γ-ray band (e.g., Fossati et al. 1998).

The source of the high-energy peak is still under debate, with models for the production of γ-ray photons classified into two broad classes: hadronic and leptonic models (e.g., Blandford et al. 2019). In hadronic models, processes such as photopion production are responsible for the γ-ray peak, while in leptonic models, the γ-ray peak is caused by inverse-Compton scattering of lower-energy photons, which can be the same synchrotron photons responsible for the low-energy peak (the "synchrotron self-Compton" model) or other components of the radiation field (the "external inverse-Compton" model, e.g., Sikora et al. 1994).

A key to distinguishing between these models is what they predict for multiwavelength observations of blazar flares. Leptonic models have been successful in explaining several observed aspects of blazars (Sikora et al. 1994; Sikora & Madejski 2003). The simplest interpretation of leptonic models predict that when observing AGN light curves in multiple wavelengths, there should be correlated variability between the synchrotron peak and the high-energy peak. This behavior has been observed in many cases (e.g., Bonning et al. 2009), but evidence exists that it may not always be present. For example, in the multiwavelength study of PKS 0208-502, an "orphan flare" was observed, in which a significant flux increase is seen in the optical/infrared bands but not in the γ-ray band (Chatterjee et al. 2013a, 2013b).

Multiwavelength studies of blazar flares have traditionally included γ-ray, X-ray, optical, infrared, and radio emission. Since millimeter-wavelength radiation is a strong tracer of synchrotron emission, observations of AGN at these wavelengths should help identify the true origin of the blazar SED. Recent studies have shown that on longer timescales, millimeter-wave variability is better correlated with γ-ray emission than optical (Meyer et al. 2019; Zhang et al. 2022), while on shorter timescales features tend to correlate more between the optical and γ-ray. This points toward the possibility of synchrotron emission produced in different regions of the blazar being responsible for the millimeter–γ-ray correlation and the optical–γ-ray correlation.

It has recently been recognized that cosmic microwave background (CMB) experiments have the potential to be used as AGN monitors (e.g., Holder et al. 2019). AGN appear as bright point sources in maps made with CMB experiments, and current CMB experiments are sufficiently sensitive to detect many AGN at a high signal-to-noise ratio (S/N) in short observations. When combined with an observing strategy that results in high-cadence observations of the same patch of sky over many years, CMB data sets are effective for AGN monitoring.

We have undertaken a pilot study of AGN variability using millimeter-wave data from SPTpol, the second-generation camera on the South Pole Telescope (SPT). The SPTpol survey enables the monitoring of tens of millimeter-bright

[52] Radio-loud AGN are generally defined as AGN with a ratio of radio (5 GHz) to optical (B-band) flux ≳ 10 (Kellermann et al. 1989).

AGN on timescales from days to years at high S/N (>10 in a 36 hr coadd). These observations provide the opportunity to include high-cadence millimeter-wave data in the study of the physical mechanisms behind AGN emission.

Although our SPTpol AGN monitoring campaign includes tens of sources, we choose to focus on the blazar PKS 2326-502 for this pilot study because of its long history of observations in multiple wavelengths (e.g., Dutka et al. 2017). PKS 2326-502 is among the targets of monitoring by both the Fermi Large Area Telescope (LAT) and Yale Small and Moderate Aperture Research Telescope System (SMARTS) Blazar Group collaborations. In particular, PKS 2326-502 has publicly available Fermi (γ-ray) and SMARTS (optical) observations over most of the time period over which we have SPTpol data.

2. Observations

In our study of PKS 2326-502, we use data from SPT, SMARTS, and Fermi-LAT. In this section, we describe the observations and data reduction for each instrument.

2.1. SPT

The SPT (Carlstrom et al. 2011) is a 10 m telescope located at the geographic South Pole and dedicated to making low-noise, high-resolution maps of the millimeter-wave sky, with the primary goal of mapping the temperature and polarization anisotropies in the CMB. Three separate cameras have been installed on the telescope, each used to map multiple large patches of the Southern Celestial Hemisphere. This work uses data from the second-generation camera, SPTpol. From 2013 to 2016 SPTpol was used during most of the year to survey 500 deg^2 of the southern extragalactic sky at arcminute resolution to mJy noise levels in bands centered at 95 and 150 GHz. The 500 deg^2 SPTpol survey consists of ~3500 observations of a field covering 22^h to 2^h in R.A. and −65° to −50° in decl. (Henning et al. 2018). For this study we take 150 GHz maps made from individual observations and combine them into 36 hr bundles, which provides a reasonable match with the cadence of other data sets while also providing high S/N on a sufficient number of sources.

Once bundle maps are created, we apply a matched filter that removes the long-wavelength modes from each map, maximizing the S/N on point sources. These filtered bundles have a 1σ error of ~9 mJy, providing us with S/N >10 on 25 AGN in the 500 deg^2 field. We perform a series of calibration and systematic checks for each bundle. We check and correct per-bundle astrometry by comparing the positions of bright sources to those in the AT20G catalog (Murphy et al. 2010). We correct the calibration of each bundle by calculating the cross-spectrum of that bundle map with the Planck 143 GHz map (Planck Collaboration et al. 2020) and scaling the bundle map so that the cross-spectrum agrees with that calculated for the average of all bundles. We additionally check for contamination in each bundle (such as from sidelobe pickup from the Sun in observations during the Austral summer, which would appear as bright streaks in our observations) by visually inspecting $5' \times 5'$ patches of sky centered on PKS 2326-502. No such contamination was detected. Once all maps have been calibrated and checked, we extract the fluxes that are used to create the millimeter-wave light curve of PKS 2326-502.

2.2. SMARTS

This paper makes use of optical/near-infrared light curves that are available at the SMARTS website.[53] The SMARTS telescope is located in Cerro Tololo Chile, and is thus well suited to monitoring of Southern Hemisphere targets. The SMARTS blazar sample was initially (in 2008) defined to include all Fermi-LAT-monitored blazars on the initial public release list with decl. <20°. Observations were made in the B, V, R, J, and K bands, with an observing cadence of 1–3 days. Here, we use the 1 day cadence optical R-band observations to match the SPT cadence as closely as possible. The full details of the data selection and analysis procedure for SMARTS data can be found in Bonning et al. (2012).

2.3. Fermi-LAT

The Fermi-LAT light curve for PKS 2326-502 is taken from the Fermi-LAT Light Curve Repository (LCR; Abdollahi et al. 2023).[54] The LCR is a public database of multicadence flux-calibrated light curves for over 1500 variable sources in the 10 yr Fermi-LAT point source catalog (4FGL-DR2; Ballet et al. 2020). The light curves generated by the LCR span the duration of the mission and are obtained by performing an unbinned likelihood analysis over the energy range 100 MeV–100 GeV. The LCR analysis uses the standard Fermi-LAT Science Tools (version v11r5p3) and the P8R2_SOURCE_V6 instrument response functions on P8R3_SOURCE class photons. Photons are selected from a 12° region of interest centered on the location of the 4FGL-DR2 counterpart of PKS 2326-502 (4FGL J2329.3-4955). A zenith angle cut of 90° is used to prevent contamination from the Earth's limb. Included in the photon distribution model used to calculate the flux of the target source are all 4FGL-DR2 point sources within 30° as well as Galactic diffuse (gll_iem_v07.fits) and isotropic (iso_P8R3_SOURCE_V3_v1) background models. The LCR provides light curves in cadences of 3 days, 1 week, and 1 month. For this analysis we use the minimum available time binning of 3 days.

3. Methods

In this Letter, we report both qualitative and quantitative results from the analysis of multiwavelength light curves of PKS 2326-502. Quantitatively, we measure the local cross-correlation functions (CCFs)[55] of year-long light curves and calculate the significance by comparing these to uncorrelated simulations. The simulations were created by taking the power spectrum of the light curve from each data set, fitting to a model in which the light-curve fluctuation power is a function of temporal frequency $P(f) = P_0(1 + (f/f_{\mathrm{knee}})^{-a})$, and producing 10,000 simulations of light curves from each model power spectrum. The simulated light curves are generated in Fourier space with random phase (i.e., they obey Gaussian statistics in real space). Some recent results have indicated that, at least in the γ-ray, blazar variability is better described by a lognormal probability distribution than a Gaussian (e.g., Duda & Bhatta 2021). We have created an alternate set of simulations with lognormal statistics and do not

[53] www.astro.yale.edu/smarts/glast/home.php

[54] https://fermi.gsfc.nasa.gov/ssc/data/access/lat/LightCurveRepository

[55] Here "local" refers to calculating the mean and variance of both light curves over individual time lag bins rather than the entire light curve; see Welsh (1999) for details.

see any significant change in our results when we use this alternate set.

We calculate the local CCF for each pair of light curves in the real data and all 10,000 simulations using the following procedure. For a given time lag bin τ, we select all data points in light curves a and b that satisfy

$$t(a) - t(b) \in \tau \pm \frac{\Delta\tau}{2}, \quad (1)$$

where Δτ is the bin width, and t(a) and t(b) are the times for observations in each light curve. We define the local CCF as

$$\mathrm{CCF}(\tau) = \frac{\sum_{i=1}^{n}(a_i - \bar{a})(b_i - \bar{b})}{(n-1)\sigma_a\sigma_b}, \quad (2)$$

where σ_a is defined as

$$\sigma_a = \sqrt{\frac{1}{n-1}\sum_{i=1}^{n}(a_i - \bar{a})^2}, \quad (3)$$

$\bar{a}$ is defined as

$$\bar{a} = \frac{1}{n}\sum_{i=1}^{n} a_i, \quad (4)$$

and i runs over all pairs of points that satisfy Equation (1). The simulated CCFs were then used to find the 1σ, 2σ, and 3σ contours for the data CCFs.

As discussed in Welsh (1999), measuring the full correlation function is challenging in data that is dominated by the longest timescale feature in the data. We also wish to remove possible dependencies on the binning timescale of any of our data sets. For these reasons, we boxcar-smooth all of the light curves with a 7 day window, and we only calculate the full CCF on data that have been detrended using a polynomial filter. We use a fifth-order polynomial per year, which preserves features up to timescales of months. For data that have not been detrended, we only calculate the zero-lag correlation and associated p-value. This p-value is estimated by calculating the number of simulations that have a higher zero-lag correlation than the data:

$$p(\mathrm{CCF}, \tau = 0) = \frac{N(\mathrm{CCF}_{\mathrm{sim}}, \tau = 0 > \mathrm{CCF}_{\mathrm{data}}, \tau = 0)}{N_{\mathrm{sims}}}. \quad (5)$$

For detrended data, we calculate this zero-lag correlation and p-value, and we further plot the full CCF and look for evidence of lags between the flaring in different bands.

4. Results

Multiwavelength (γ-ray, optical, millimeter-wave) light curves for 4 yr of monitoring of PKS 2326-502 are shown in Figure 1. We note that the raw statistical significance of the variability in all three bands is high: the typical S/N in a single 36 hr SPT light-curve point is ~50 in the quiescent state and over 200 in the flaring state, and the corresponding S/N for the 3 day Fermi light-curve points are 1–2 and 7–10. For SMARTS-R, where we only have data in the flaring state, the typical S/N per 1 day point is ~50.

Several features of these light curves that make up the primary results of this Letter are evident by eye in Figure 1, including the following:

1. A long-timescale flaring state in the first 2 yr followed by a 2 yr quiescent period.
2. Long-timescale correlation between millimeter-wave and γ-ray data, with the millimeter-wave light curve appearing to decay more slowly than the γ-ray one.
3. Short-timescale correlation between γ-ray and optical data.

For our quantitative analyses, we focus on the observations made in the first 2 yr of available SPTpol data (2013–2014), because (1) PKS 2326-502 entered into a quiescent state thereafter, and (2) there are no publicly available optical data from SMARTS after 2014. For all possible pairs of data, two sets of light curves (boxcar-smoothed and smoothed-and-detrended) and CCFs for the smoothed and detrended data are shown for year 1 and year 2 in Figures 2 and 3 respectively.

As a rough measure of the significance of the correlated year timescale flare in the γ-ray and millimeter-wave bands, we calculate the number of simulations that show a similar or larger flux increase over 1 yr in those two bands. We find that only 42 out of 10,000 simulations show a factor of 2.5 increase over 1 yr in both bands. We chose a factor of 2.5 because the ratio of the flux in the first and last month of year 1 was 2.7 in SPT and 3.3 in Fermi. Therefore, we report 4.2×10^{-3} as a raw, non-trials-corrected p-value for this long-timescale correlated flaring state. We also calculate the zero-lag correlation for the unfiltered boxcar-smoothed year-1 data and we find a zero-lag correlation value of 0.75 for SPT × Fermi. Only 287 simulations show a zero-lag correlation between SPT × Fermi higher than this; thus, we report in Table 1 a p-value of 0.03 for this correlation.

Another fairly strong identifiable feature in the data is the short ~week-timescale flare seen in both Fermi and SMARTS but not in SPT. This leads to a significant detection of zero-lag correlation even in the nondetrended data p(CCF, τ = 0) = 3×10^{-4}. Once we filter out the long-timescale features we find a zero-lag correlation value much higher than found in any of our simulations and thus report a p-value of $<10^{-4}$ in Table 1. This confirms that this correlation is being driven by the shorter-timescale feature in the Fermi and SMARTS light curves shown in Figure 2. By contrast, when we detrend SPT × Fermi data in year 1, we find no evidence of correlation on shorter timescales.

In contrast to year 1, for year 2 we find a significant correlation between the detrended SPT × Fermi light curves, but none for the SMARTS × Fermi light curves, as shown in Figure 3. We also find no significant correlation between any of the data sets in year 2 prior to detrending. Finally we note that we measure no significant correlation at nonzero lag for any data combination in either year.

5. Discussion

Our study of the multiwavelength variability of PKS 2326-502 yields four primary results:

1. Long-timescale correlation between millimeter-wave and γ-ray data, with the millimeter-wave light curve appearing to decay more slowly than the γ-ray one.

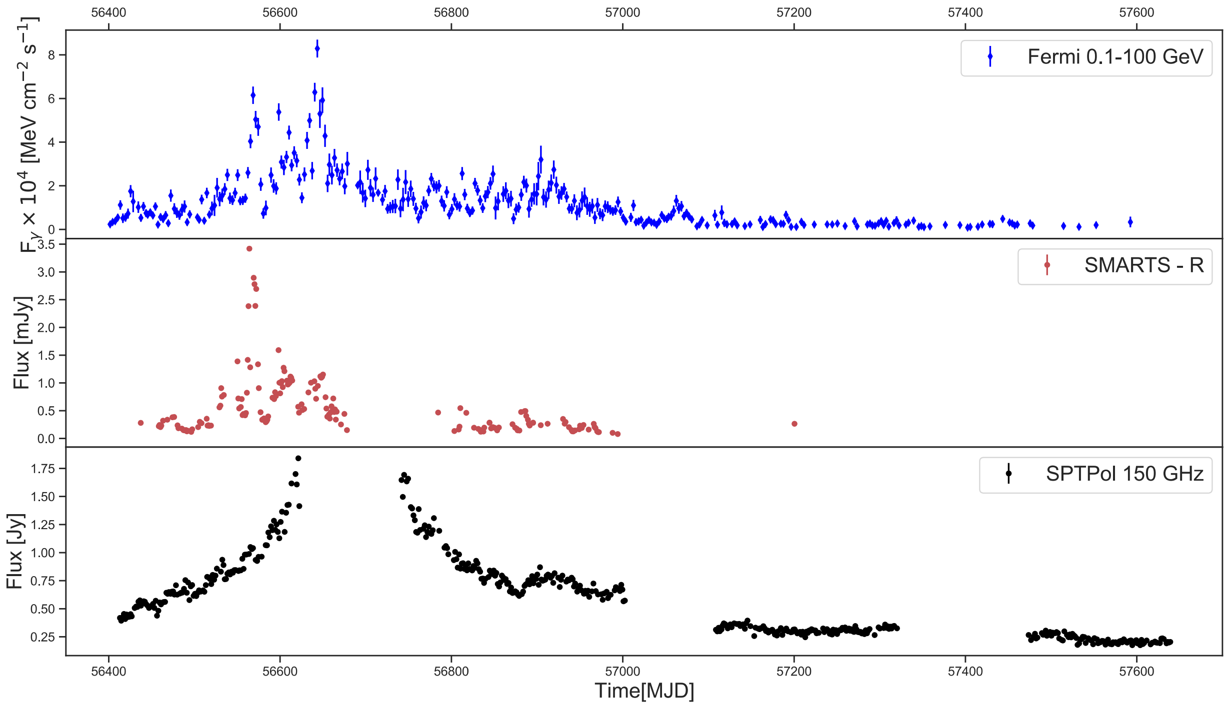

Figure 1. Light curves for PKS 2326-502. Top: Fermi-LAT. Middle: SMARTS optical R. Bottom: SPTpol 150 GHz. Evident by eye are long-timescale correlation between millimeter-wave and γ-ray observations and short-timescale correlation between optical and γ-ray observations. For reference, MJD 56,400 was calendar 2013 April 18. The time gaps in the SPTpol data are periods during the austral summer when the primary 500 deg^2 field was not observed to avoid solar contamination.

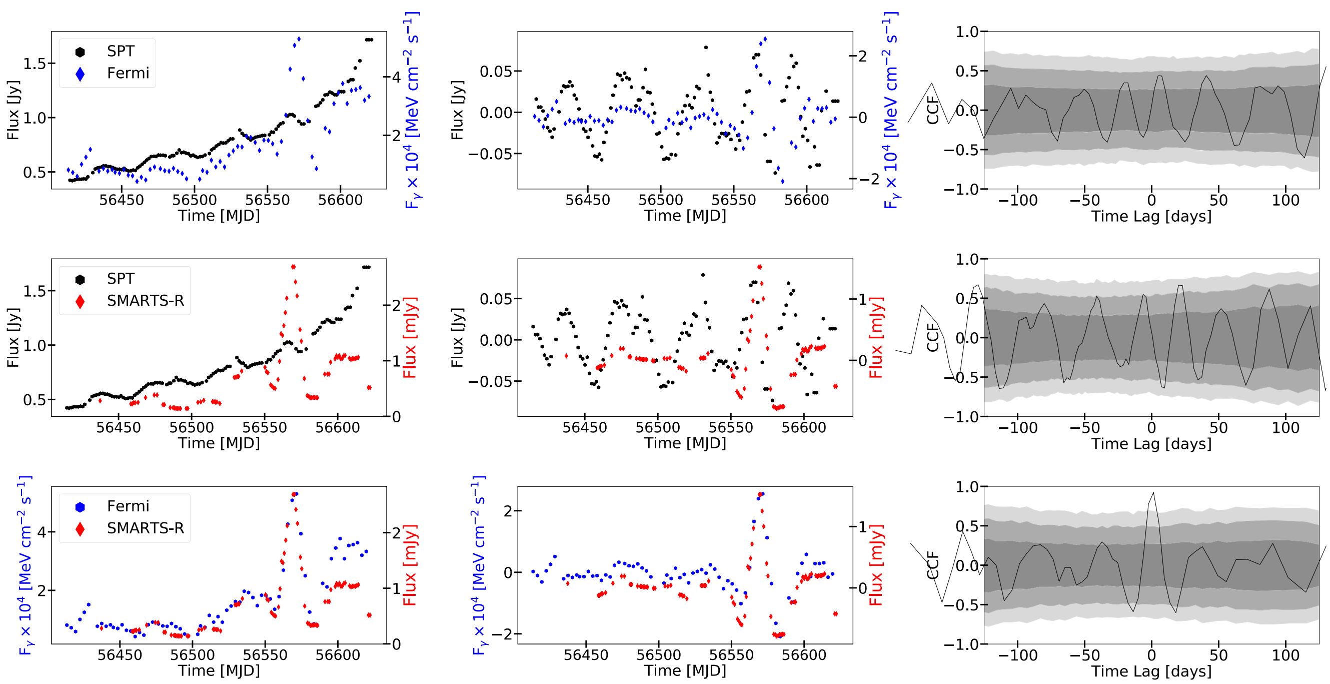

Figure 2. Year-1 boxcar-smoothed light curves (left column), smoothed and detrended light curves (middle column), and detrended CCFs (right column). The gray shaded regions represent the 1σ, 2σ, and 3σ contours of simulated CCFs.

2. Short-timescale correlation between γ-ray and optical light curves in year 1.
3. Short-timescale correlation between γ-ray and millimeter-wave light curves in year 2.
4. No measurable correlation between millimeter-wave and optical light curves.

These results have implications for the production mechanism of γ-rays in blazars and the structure of these systems in general. Very broadly, the correlated variability we observe between the γ-ray light curves and those in the optical and millimeter-wave is more consistent with leptonic models of γ-ray production than with hadronic models. While a quantitative

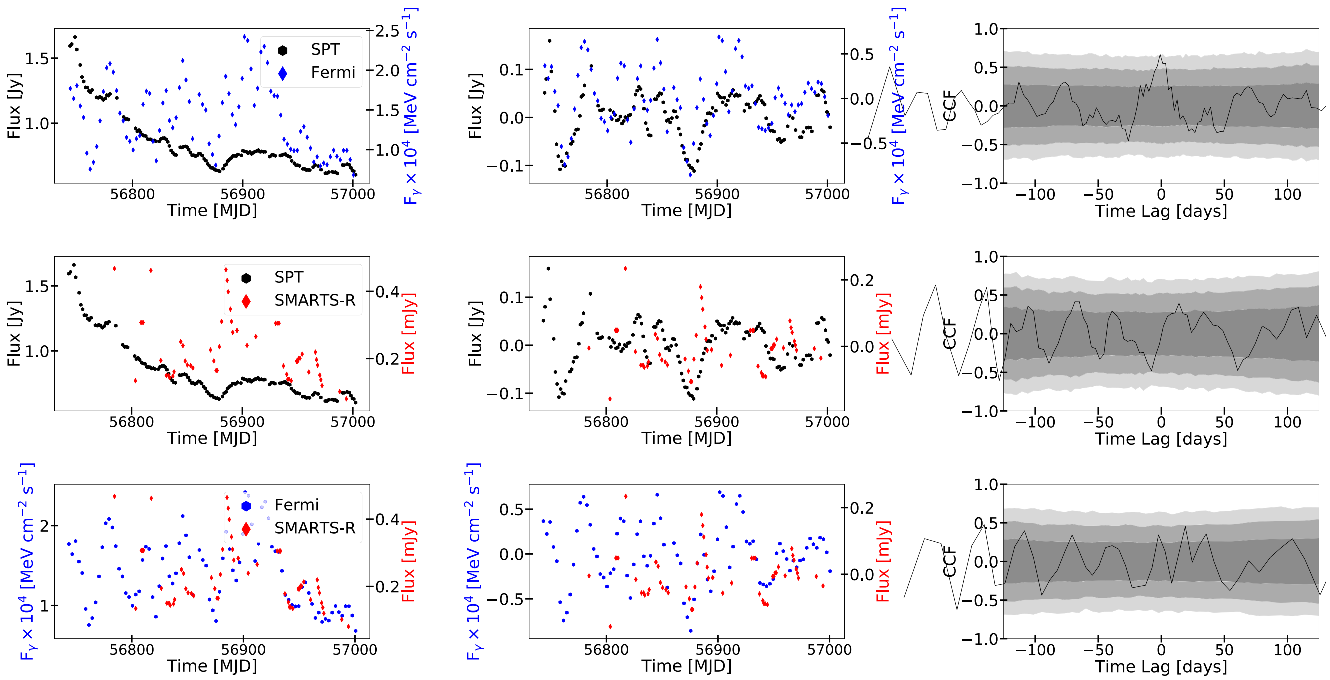

Figure 3. Same as Figure 2 but for year 2.

Table 1
Values of Zero-lag Correlation and Associated p-value for Smoothed and Smoothed-and-detrended Data

Light-curve Statistics		
Data Set	Zero-lag Correlation	Zero-lag p-value
SPT × Fermi year 1 (smoothed)	0.75	2.9×10^{-2}
SPT × Fermi year 1 (smoothed and detrended)	-1.3×10^{-2}	0.52
Smarts × Fermi year 1 (smoothed)	0.92	3.0×10^{-4}
Smarts × Fermi year 1 (smoothed and detrended)	0.92	$<10^{-4}$
SPT × Smarts year 1 (smoothed)	0.48	0.16
SPT × Smarts year 1 (smoothed and detrended)	2.6×10^{-2}	0.47
SPT × Fermi year 2 (smoothed)	0.23	0.32
SPT × Fermi year 2 (smoothed and detrended)	0.67	1.0×10^{-3}
Smarts × Fermi year 2 (smoothed)	0.54	7.4×10^{-2}
Smarts × Fermi year 2 (smoothed and detrended)	0.34	8.7×10^{-2}
SPT × Smarts year 2 (smoothed)	0.32	0.26
SPT × Smarts year 2 (smoothed and detrended)	9.7×10^{2}	0.36

Note. Values for years 1 and 2 are reported separately.

comparison of our findings with predictions of specific leptonic models are beyond the scope of this paper, we note that simple scaling arguments predict that, in the external inverse-Compton model, the fractional amplitude of a γ-ray flare should scale linearly with the synchrotron flare amplitude. On the other hand, in the synchrotron self-Compton model, the γ-ray flare amplitude should be roughly the square of that seen in synchrotron. The long-timescale flare in year 1 is of similar fractional amplitude in the millimeter-wave and γ-ray data, lending some support to the external model. We also note the longer lifetime of the millimeter-wave outburst is consistent with a longer radiative lifetime of millimeter-wave electrons as discussed in, e.g., Potter (2018).

Independent of the production of γ-rays, a puzzling feature of our data is the complete lack of correlation between the optical and millimeter-wave data. For year 1, a possible explanation for this lack of correlation is that we are seeing different regions of the jet in the two bands because the millimeter-wave synchrotron radiation is optically thick. This would also be consistent with the long-timescale correlation between the millimeter-wave and γ-ray light curves and the short-timescale correlation of γ-ray and optical light curves, because we would expect to see short-timescale variability only closer to the central black hole. In this picture, the short-timescale millimeter-wave and γ-ray correlation in year 2 is consistent with the millimeter-wave radiation becoming optically thin. This motivates the comparison of millimeter-wave optical thickness at different points in the light curve. To explore this, we extract 95 GHz SPTpol fluxes for PKS 2326-502 in a subset of observations, using procedures identical those used to extract the 150 GHz flux (Section 2.1). We measure the millimeter-wave spectral index, which we define through

$$S_\nu \propto \nu^{\alpha}; \qquad (6)$$

i.e., we estimate α as

$$\alpha = \frac{\ln\left(\frac{S_{150}}{S_{95}}\right)}{\ln\left(\frac{\nu_{150}}{\nu_{95}}\right)}, \qquad (7)$$

where S_{95} and S_{150} are the 95 and 150 GHz fluxes, and ν_{95} and ν_{150} are the effective band centers for a synchrotron source. We estimate α for four 36 hr bundles, each near the three prominent features in the millimeter-wave light curve: the peak of the long-timescale flare in year 1, the short-timescale flare in year 2, and the quiescent period in year 3.

We find values of the millimeter-wave spectral index of α = −0.24 at the peak of the year-1 flare, α = −0.52 in the year-2 flare, and α = −0.95 in the quiescent period. These values are consistent with the picture of the millimeter-wave optical thickness decreasing after the year-1 flare peaks, thus allowing us to see farther upstream in the millimeter-wave in year 2 than in year 1. What this scenario does not explain is why we do not see any correlation between the optical and millimeter-wave radiation in year 2. It is possible that the optical synchrotron radiation tracing this activity is too faint, and that any variation in the optical flux in year 2 is caused by an unassociated process.

6. Conclusion

We have presented results from a pilot study using CMB data to monitor AGN, in particular the blazar PKS 2326-502. We have correlated the millimeter-wave light curve from SPTpol with γ-ray data from Fermi-LAT and optical data from SMARTS. We measured long- and short-timescale correlation between the millimeter-wave and γ-ray light curves and short-timescale correlation between the optical and γ-ray light curves, but we found no measurable correlation between the millimeter-wave and optical light curves. These results are broadly consistent with leptonic models of γ-ray production in blazars, but they imply that the production of synchrotron emission is more complex than a single source at all wavelengths.

While this study only used data from a single object, we have millimeter-wave data from many more AGN in the SPTpol survey that we will use in future investigations of multi-wavelength correlation. We will further expand this monitoring program using the yet more sensitive data from the current camera on the SPT, SPT-3G (Sobrin et al. 2022). Future experiments such as Simons Observatory (Simons Observatory Collaboration et al. 2019) and CMB-S4 (CMB-S4 Collaboration et al. 2019) will cover up to 70% of the sky at nearly daily cadence with similar or even higher sensitivity. These large-footprint, high-cadence CMB surveys will be particularly well suited for correlation with optical monitoring from VRO-LSST (Ivezić et al. 2019). CMB experiments are poised to become an integral part of the AGN monitoring landscape.

The South Pole Telescope program is supported by the National Science Foundation (NSF) through awards OPP-1852617 and OPP-2147371. Partial support is also provided by Vanderbilt University and the Kavli Institute of Cosmological Physics at the University of Chicago. J.H. acknowledges support from the NSF through award OPP-2219065.

Facilities: SPT, FERMI, SMARTS.

ORCID iDs

J. C. Hood II https://orcid.org/0000-0003-4157-4185
A. McDaniel https://orcid.org/0000-0002-8436-1254
A. Foster https://orcid.org/0000-0002-7145-1824
P. A. R. Ade https://orcid.org/0000-0002-5127-0401
M. Ajello https://orcid.org/0000-0002-6584-1703
J. E. Austermann https://orcid.org/0000-0002-6338-0069
J. A. Beall https://orcid.org/0000-0003-1263-6738
A. N. Bender https://orcid.org/0000-0001-5868-0748
B. A. Benson https://orcid.org/0000-0002-5108-6823
F. Bianchini https://orcid.org/0000-0003-4847-3483
L. E. Bleem https://orcid.org/0000-0001-7665-5079
J. E. Carlstrom https://orcid.org/0000-0002-2044-7665
T. M. Crawford https://orcid.org/0000-0001-9000-5013
M. A. Dobbs https://orcid.org/0000-0001-7166-6422
W. Everett https://orcid.org/0000-0002-5370-6651
E. M. George https://orcid.org/0000-0001-7874-0445
N. Gupta https://orcid.org/0000-0001-7652-9451
G. P. Holder https://orcid.org/0000-0002-0463-6394
A. T. Lee https://orcid.org/0000-0003-3106-3218
M. Malkan https://orcid.org/0000-0001-6919-1237
S. Patil https://orcid.org/0000-0001-5871-7520
C. Pryke https://orcid.org/0000-0003-3983-6668
C. L. Reichardt https://orcid.org/0000-0003-2226-9169
G. Smecher https://orcid.org/0000-0002-5560-187X
A. A. Stark https://orcid.org/0000-0002-2718-9996
J. D. Vieira https://orcid.org/0000-0001-7192-3871
N. Whitehorn https://orcid.org/0000-0002-3157-0407
W. L. K. Wu https://orcid.org/0000-0001-5411-6920
L. Zhang https://orcid.org/0000-0003-0232-0879

References

Abazajian, K., Addison, G., Adshead, P., et al. 2019, arXiv:1907.04473
Abdollahi, S., Ajello, M., Baldini, L., et al. 2023, arXiv:2301.01607
Antonucci, R. 1993, ARA&A, 31, 473
Ballet, J., Burnett, T. H., Digel, S. W., & Lott, B. 2020, arXiv:2005.11208
Blandford, R., Meier, D., & Readhead, A. 2019, ARA&A, 57, 467
Bonning, E. W., Bailyn, C., Urry, C. M., et al. 2009, ApJL, 697, L81
Bonning, E., Urry, C. M, Bailyn, C., et al. 2012, ApJ, 756, 13
Carlstrom, J. E., Ade, P. A. R, Aird, K. A, et al. 2011, PASP, 123, 568
Chatterjee, R., Nalewajko, K, Myers, A. D, et al. 2013a, ApJL, 763, L11
Chatterjee, R., Nalewajko, K., & Myers, A. D. 2013b, ApJL, 771, L25
Duda, J., & Bhatta, G. 2021, MNRAS, 508, 1446
Dutka, M. S., Carpenter, B. D., Ojha, R., et al. 2017, ApJ, 835, 182
Fossati, G., Maraschi, L., Celotti, A., Comastri, A., & Ghisellini, G. 1998, MNRAS, 299, 433
Gebhardt, K., Bender, R., Bower, G., et al. 2000, ApJL, 539, L13
Henning, J. W., Sayre, J. T., Reichardt, C. L., et al. 2018, ApJ, 852, 97
Holder, G., Berger, E., Bleem, L., et al. 2019, BAAS, 51, 331
Ivezić, Ž., Kahn, S. M., Tyson, J. A., et al. 2019, ApJ, 873, 111
Kellermann, K. I., Sramek, R., Schmidt, M., Shaffer, D. B., & Green, R. 1989, AJ, 98, 1195
Kormendy, J., & Richstone, D. 1995, ARA&A, 33, 581
Meyer, M., Scargle, J. D., & Blandford, R. D. 2019, ApJ, 877, 39
Murphy, T., Sadler, E. M., Ekers, R. D., et al. 2010, MNRAS, 402, 2403
Planck Collaboration, Aghanim, N., Akrami, Y., et al. 2020, A&A, 641, A1
Potter, W. J. 2018, MNRAS, 473, 4107
Sikora, M., Begelman, M. C., & Rees, M. J. 1994, ApJ, 421, 153
Sikora, M., & Madejski, G. M. 2003, in ASP Conf. Ser. 290, Active Galactic Nuclei: From Central Engine to Host Galaxy, ed. S. Collin, F. Combes, & I. Shlosman (San Francisco, CA: ASP), 287

Simons Observatory Collaboration, Ade, P., Aguirre, J., et al. 2019, JCAP, 2019, 056
Sobrin, J. A., Anderson, A. J., Bender, A. N., et al. 2022, ApJS, 258, 42
Urry, C. M., & Padovani, P. 1995, PASP, 107, 803
Welsh, W. F. 1999, PASP, 111, 1347
Zhang, L., Vieira, J. D., Ajello, M., et al. 2022, ApJ, 939, 117